Carbon, Captured: 1D Reactive Transport Modelling of NCG reinjection in Mt Apo Geothermal Production Field

Fredeve John Pacatang[1], Eylem Kaya[2]

[1]Energy Development Corporation, 6th Floor Rockwell Business Center Tower 3, Ortigas Avenue, Pasig City, Philippines

[2]The Department of Engineering Science and Biomedical Engineering, University of Auckland, 70 Symonds St, Auckland, New Zealand

pacatang.fjp@energy.com.ph and e.kaya@auckland.ac.nz

ABSTRACT

This study presents a one-dimensional (1D) radial model to investigate the reactive transport behavior in the Mt Apo Geothermal Production Field, focusing on Well K1's major feedzone, subject to various reinjection scenarios including neutral brine, binary brine, and a proposed non-condensable gas (NCG)-charged binary brine using TOUGHREACT v4.13 EOS 1. It explores the geochemical and mineralogical changes induced by NCG-charged fluid injection under reservoir conditions. The simulation captures key processes such as dissolution, mineral alteration, and secondary mineral precipitation within the feedzone-to-reservoir flow path. The 1D model results provided insights into potential impacts on injectivity and showed permeability enhancement due to thermal effects, with calcite, dolomite, epidote, illite, and anhydrite undergoing consistent dissolution at different magnitudes under low-pH injection. This 1D modelling approach offers an informative guide for field-scale predictions and supports the development of an effective NCG-geothermal wastewater mixture injection strategies for geothermal reservoir management.

Keywords: Fluid-rock interaction, reactive transport modelling, TOUGHREACT, CO_2, geothermal reinjection.

1. INTRODUCTION

Geothermal energy is one of the energy sources that we can harness primarily for power production and direct use. Although renewable, it is not free from greenhouse gas emissions as production of non-condensable gases (e.g., CO_2, H_2S, H_2, NH_3, CH_4) are inherent when dealing with hydrothermal systems (Altar and Kaya, 2020). The recent global estimate of GHG emissions from geothermal is averaging at 122 gCO_2/kWh (Fridriksson, 2017). In the Philippines, EDC reported to have around 105 gCO_2/kWh emission on its combined geothermal capacity nationwide in 2023. This is significantly lower than coal, oil, and natural gas (DOE, 2023). While geothermal's carbon dioxide emissions are slightly higher than wind, solar, and hydro, it is still within the "low carbon" category (McClean and Richardson, 2024).

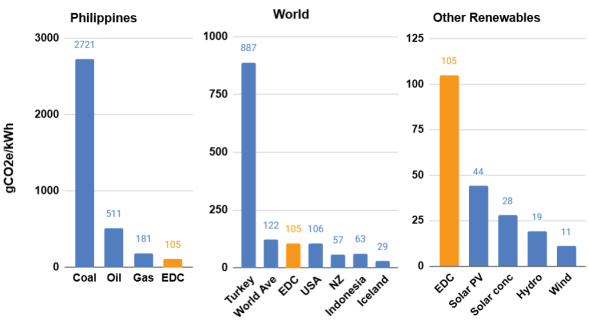


Figure 1. (a) GHG Emissions From Fossil Fuels and EDC (b) Worldwide Geothermal Emission Comparison (c) Comparison to Other Renewables.

1.1 NCG reinjection worldwide comparison

An emerging method to reduce GHG emissions from geothermal is through co-injection where NCG is mixed with the

condensate or brine for reinjection back into the reservoir. Several countries such as Iceland (Sigfusson et al., 2018; Ratouis et al., 2022), Turkey (Erol et al., 2022; Yucetas et al., 2018), Japan (Yanagisawa, 2010; Kaieda et al., 2009), USA (Adams et al., 2000) and New Zealand (Ruiz et al., 2021; McClean and Richardson, 2024; Abd Ghafar et al., 2022) have been doing this; however, each geothermal field has unique characteristics and may have different response to this reinjection scheme. Some of these projects have reported problems like scaling in production lines, NCG breakthrough to adjacent production wells, and increased operational costs (Siahaan, 2024).

Table 1. Comparison of Different Geothermal Fields with NCG reinjection.

Site	Rock type	Year started	Amount CO_2 injection	Issues encountered / Notable Results
Hellisheidi/Nesjavellir, Iceland (Ragnarsdottir et al., 2023; Levy et al., 2021)	Basalt	2014	12 Mt/yr CO_2 6 Mt/yr H_2S	Mineralization occurred in reservoir
Ogachi/Hiroji, Japan (Ueda et al., 2010; Kaieda, 2021)	Granite (EGS)	2007	1% w/w CO_2 (dry ice)	Calcite precipitation
Umurlu, Turkey (Yucetas et al., 2018)	Carbonate	2017	1.2 Mt CO_2 for 20 days	CO_2 breakthrough in production wells
Kizildere, Turkey (Sevindik et al., 2024)	Carbonate	2022	985 tCO_2 for 6 months	No CO_2 increase in produced fluid
Ngā Tamariki, New Zealand (Abd Ghafar et al., 2022)	Greywacke	2022	100% reinjection (3/4 units)	No scaling/NCG changes in production wells
Te Huka, New Zealand (Richardson et al., 2023)	Greywacke	2011-partial	100% reinjection (2022)	No issues regarding gas breakout
Coso, USA (Kolar et al., 2015)	Granite	1989	H_2S injection	High maintenance cost
Puna, USA (Bonafin et al., 2019; DePippo, 2016)	Basalt	1984	Total fluid and gas reinjection	No issue on corrosion

In the Philippines, there's no NCG reinjection that has been operationally done yet among the geothermal fields except for the pilot testing conducted in Tongonan-I in 2005 (Villena et al., 2005). For this study, the Mindanao Geothermal Production Field located in Mt Apo is considered. It was originally composed of two units (Mindanao 1 and Mindanao 2) with a 701-hectare concession and 104 MW capacity which started production in 1997. In 2022, a third power plant was commissioned (Mindanao 3 Binary) with a 3.6 MW capacity utilizing the separated brine from Mindanao 1 (Frassinetti et al., 2022). With the lower brine temperature at the outlet of the binary plant, it increases the scaling potential down the reinjection wells. Hence, this study aims to investigate the effect of mixing non-condensable gases to the brine and to check the changes in porosity, permeability, mineral volume fraction, chemistry, and other parameters around the reinjection well using the 1D radial model.

1.2 Well K1 in Mt Apo Geothermal Production Field

Well K1 is one of the reinjection wells in the Mindanao Geothermal Production Field located in Mt Apo. The field is geographically divided into three sectors: Matingao-Kullay, Marbel, and Sandawa; the latter two sectors are feeding the flash power plants (Mindanao 1 and 2) while the former serves as the injection sink (Aragon and Sambrano, 2010; Malibiran and Zarrouk, 2014) (see Figure 2).

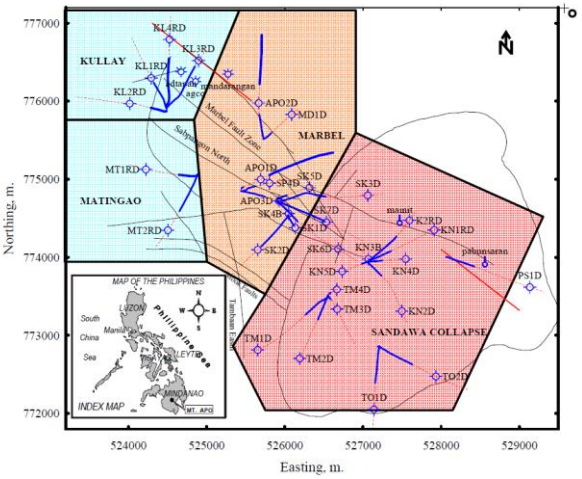


Figure 2. Map of MGPF Showing Geographical Boundaries (Aragon & Sambrano, 2010).

The feedzones of Well K1 as viewed in Leapfrog is shown in Figure 3. Well K1 was originally one of the hot reinjection wells in the Kullay sector before it was dedicated to the binary operations. It was drilled in the outflow region with a shallow major feed zone (at around 114mRSL with 40m thickness) along with four more permeable zones at greater depths. It intersects three structures, namely N-NW Sisiman, Sisiman Splay, and Sisiman Fault at depths of 175 to -625mRSL (Sambrano et al., 2010).

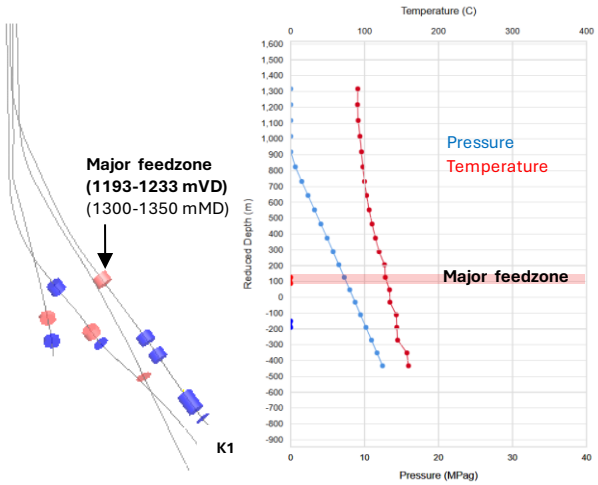


Figure 3. Well K1's Feedzones and Shut Pressure and Temperature Plot.

2. METHODOLOGY

2.1 1D Model Setup

A 1D radial model grid was generated using PyTOUGH scripts with only one layer at 40m thickness to match Well K1's major feedzone contributing 50% of the total flow rate (see Figure 3). It was set up with a 0.1 m well radius (removed from the blocks) and the next 3.338 m as skin zone, another zone up to 2049 m for the reservoir, and extended up to 28.5 km representing the outer reservoir boundary as shown in Figure 4. The block sizes were increasing logarithmically and the last gridblock was made large enough to accommodate the fluid flow and avoid boundary effects. MINC approach was used to setup the skin and reservoir zone up to 2049m with 98% matrix and 2% fracture volume fraction because the nearest production well feedzone is at around 2000 m from the injection feedzone being modelled, while the outer reservoir boundary layer was only set as single porosity.

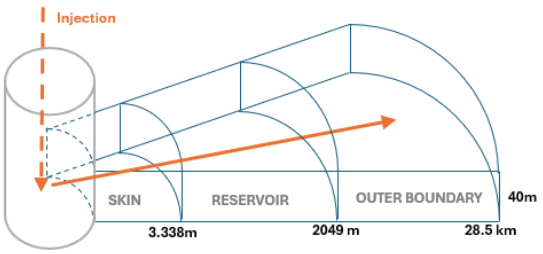


Figure 4. Unscaled Illustration of the 1D Radial Model.

2.2 Reactive Surface Areas

The reactive surface areas for the fracture and matrix were calculated using the equations given in the TOUGHREACT manual (Sonnenthal et al., 2018).

$$A = \frac{\pi A_{f-m}}{2\varphi_f} \qquad (Eqn\ 1)$$

$$RSA = A\,V_{frac} \qquad (Eqn\ 2)$$

For the fracture, Equation 1 above was used to get the reactive surface area where $\pi/2$ serves as the roughness factor, $A_{f\text{-}m}$ is the fracture-matrix interface area/volume ratio (considering the 98% matrix, 2% fracture setup), and ϕ_f is the true fracture porosity, then taking the RSA per mineral using Equation 2.

$$A = \frac{0.5}{r} \qquad (Eqn\ 3)$$

For the matrix, a simple cubic packing of 8 spheres was assumed and dividing the total area by the cube volume results in Equation 3. The radius is assumed to be 5.00E-04, then the same process is taken for the RSA per mineral as in Equation 2. The RSA used in the model is divided by 1000 because based on the compiled kinetic models they are usually 10-1000 times lower than the calculated (White and Peterson, 1990). Shown in Table 2 are the mineral volume fractions and calculated reactive surface areas used in the model.

Table 2. Mineral Volume Fractions and RSA of Well K1's major Feedzone.

Mineral	Volume fraction	Fracture		Matrix	
		RSA	RSA/1000**	RSA	RSA/1000**
Hematite	0.092783	1.09E+03	1.09E+00	18.55670	1.856E-02
Chlorite	0.185567	2.19E+03	2.19E+00	37.11340	3.711E-02
Goethite	0.072165	8.50E+02	8.50E-01	14.43299	1.443E-02
Smectite	0.072165	8.50E+02	8.50E-01	14.43299	1.443E-02
Calcite	0.164948	1.94E+03	1.94E+00	32.98969	3.299E-02
Dolomite	0.164948	1.94E+03	1.94E+00	32.98969	3.299E-02
Quartz	0.072165	8.50E+02	8.50E-01	14.43299	1.443E-02
Illite	0.025773	3.04E+02	3.04E-01	5.15464	5.155E-03
Epidote	0.051546	6.07E+02	6.07E-01	10.30928	1.031E-02
Am silica* **	0.000001	1.00E-03	1.00E-06	1.00E-03	1.00E-06
Anhydrite* **	0.000001	1.00E-03	1.00E-06	1.00E-03	1.00E-06

***RSA/1000 used in the model input*
****added in the model input to check if there is precipitation*

2.3 Fluid Chemistry and Reaction Kinetics

Data from drilling geology, injection and reservoir chemistry, and feed zone parameters were collected and processed to generate the input for the chemical, flow, and solute files used for TOUGHREACT. The rock parameters used for the model setup were derived from the existing 3D reservoir model but with modified porosity and permeability upon rendering very high pressures during calibration.

Three periods in sequence were modelled. The first 23 years being neutral brine injection only (Scenario 1). After that are 2 years of binary utilization (Scenario 2), where the brine is dosed with acid and injected at a lower temperature. Then three future scenarios of 10 years forecast for those mixed with CO2 co-injection—Mindanao 1 and Mindanao 2 NCG mixing with the binary brine (Scenarios 3a and 3b), and lastly the continued binary brine injection (Scenario 3c). Since no actual geochemistry data are available for the future scenarios, SOLVEQ-XPT and CHIM-XPT were used to simulate the mixing process of the binary brine and NCG from the respective steamline gas chemistry.

Meanwhile, the dissolution and precipitation of minerals are kinetically controlled, and the kinetic rates (r_n) are a product of the rate constant (k_n) and reactive surface area (A_n) with factors for mineral saturation (Ω) as shown in Equation 4 (Sonnenthal et al., 2021). A positive value means dissolution while negative indicates precipitation.

$$r_n = \pm k_n A_n \left|1 - \Omega_n^{\theta}\right|^n \qquad (Eqn\ 4)$$

The kinetic rate constants are usually reported at 25 °C, hence this is converted to the desired temperature using Equation 5 (Sonnenthal et al., 2021).

$$k_n = k_{25} \exp\left[\frac{-E_a}{R}\left(\frac{1}{T} - \frac{1}{298.15}\right)\right] \qquad (Eqn\ 5)$$

All the parameters in equations 4 and 5 are summarized in Table 4 taken from the compiled comprehensive report of Palandri and Kharaka (2004).

Table 4. Kinetic Reaction Parameters for Minerals.

Minerals	Dissolution / Precipitation	
	log k_{25}	E_a
Hematite	-14.6	66.2
Chlorite	-12.52	88
Goethite	-7.94	86.5
Smectite	-12.78	35
Calcite	-8.79	41.87
Dolomite	-8.6	95.3
Quartz	-13.98	87.7
Illite	-12.6	14
Epidote	-11.99	70.7
Am silica	-7.98 / -9.42	39 / 49.8
Anhydrite	-3.19 / 1.11	14.3 / 60.2

3. RESULTS AND DISCUSSIONS

3.1 1D Radial Model Calibration

The model was calibrated using downhole pressure to reflect the flowing or continuous injection condition observed in the field, however, there are limited shut and flowing surveys conducted on Well K1. The actual downhole pressure collected is recorded at 8.6 MPa when the well is at shut condition while 12.8 MPa at flowing condition. Nevertheless, the modelled pressure at around 12 MPa (Scenarios 1 to 3a/b/c) gives a reasonable match with the actual data while the shut pressure reflects the reservoir's static pressure (see Figure 5).

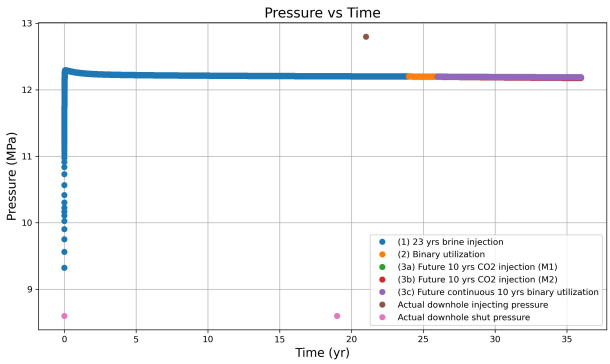


Figure 5. Modelled pressure over time with actual downhole pressures.

To validate the chemical behavior, the chemistry at the first gridblock (nearest the wellbore) was also calibrated to see if the model is giving similar results to that of the actual injected chemistry on the well (see Figure 6). The actual chemistry is from the surface and analyzed at lab conditions, so it was run with WATCH software to increase its temperature to 140°C for comparison to the model results. Based on the sulfate and silica plots, there is a good match in the model and the actual chemistry. Constant injection flow rate was implemented in the model hence a very linear modelled chemistry is reflected per period. The injection fluid pH drop after binary utilization due to the acid dosing in the brine to avoid scaling with its lower temperature reinjection was also matched with the model.

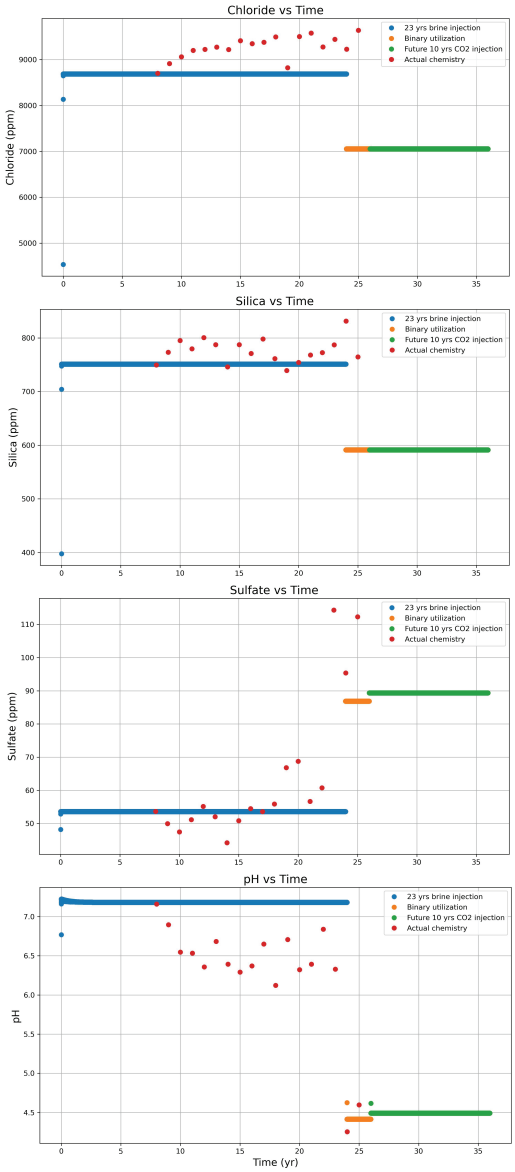


Figure 6. Modelled and Actual Chemistry Comparison Over Time.

3.2 1D Permeability and Porosity Changes

The extent of permeability changes is significant up to the skin and reservoir zone only for the fracture as shown in Figure 7 and no changes all throughout for the matrix (see Figure 7).

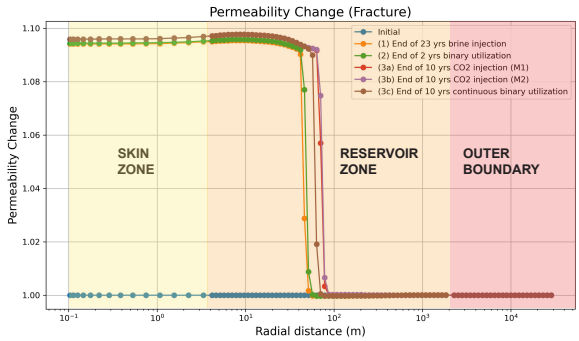


Figure 7. Permeability changes in the fracture.

Both the fracture skin and reservoir zone's permeability exhibited an increase after 23 years of brine injection and further enhancement was observed during binary utilization and the mixed CO_2 injection forecast. The maximum increase in fracture's permeability reached approximately 10% but localized only up to around 60m to 80m radial distance, beyond this zone there is no significant change observed. The permeability change in the fracture also reflects in the changes in mineral volume fractions.

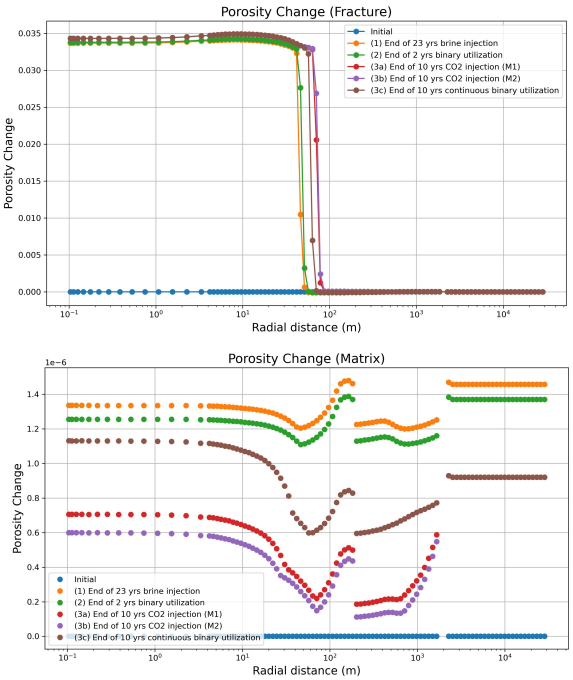


Figure 8. Porosity changes in the (a) fracture and (b) matrix.

Porosity has less pronounced changes than permeability for both the fracture and the matrix as shown in Figure 8. Although, the same trend is observed where fracture porosity change (3.5% maximum increase) is higher than the matrix (0.00014% maximum increase). Hence mineral volume fraction changes are more apparent in the fracture. The extent of porosity changes in the fracture is only up to around 60m to 80m consistent with that of permeability changes, while changes in the matrix are seen up to the outer reservoir boundary. Despite its greater radial extent, the magnitude of the matrix porosity changes is very small, and it has little to negligible manifestation in the matrix's mineral volume fraction changes.

3.3 1D Mineral Volume Fraction Changes

Given that there are higher changes in the fracture in terms of permeability and porosity, the mineral volume fraction changes are also more evident in the fracture than that in the matrix.

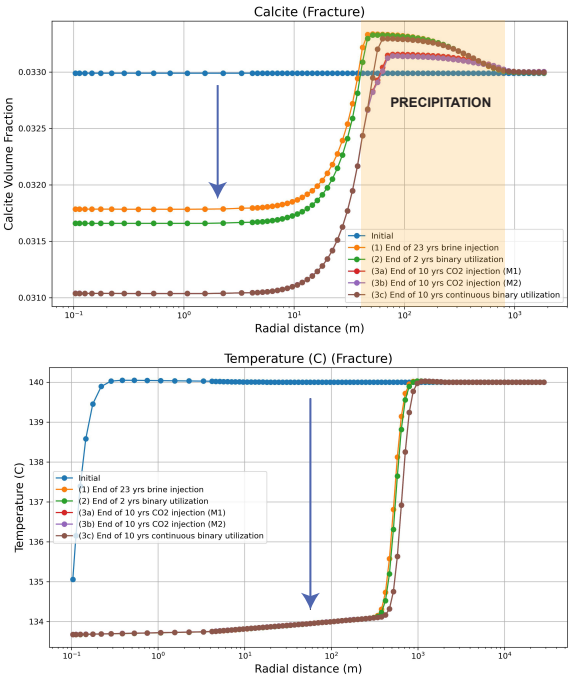


Figure 9. (a) Calcite volume fraction and (b) temperature changes across the radial distance.

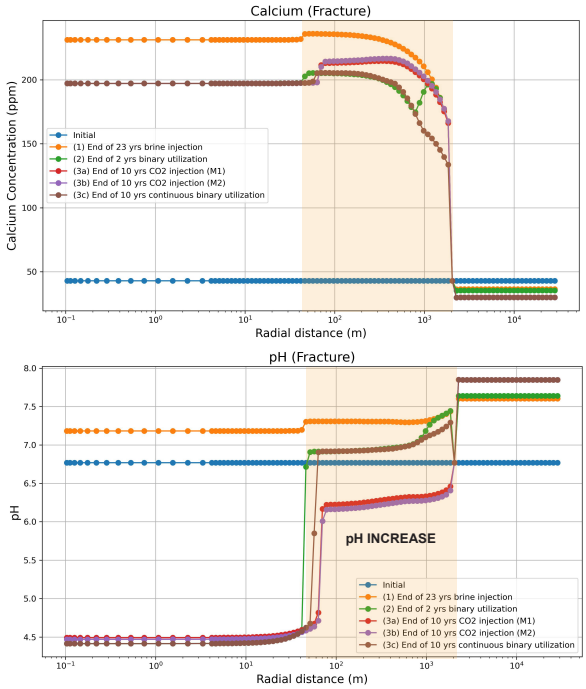


Figure 10. (a) Calcium concentration and (b) pH across the radial distance.

Calcite reaction rates are set to be kinetically controlled in the model. Calcite has a retrograde solubility, the temperature drop shown in Figure 9b promotes a slight dissolution hence a decrease in mineral volume fraction up to 3.61% following prolonged injection of neutral brine (Scenario 1). This also manifests in the increase of calcium and bicarbonate concentration in the fluid as a product of calcite dissolution. At around 25m, there is an increase in pH which coincides to a localized precipitation of calcite as it favors a more basic environment for deposition.

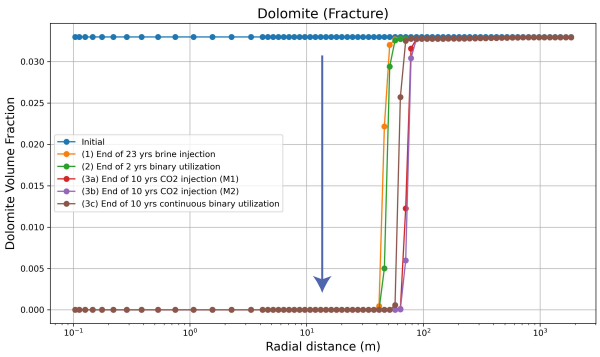


Figure 11. Dolomite volume fraction changes across the radial distance.

As for dolomite, there is a complete dissolution from the near wellbore up to around 70m for all the scenarios considered (see Figure 11). Like calcite, dolomite also has retrograde solubility and readily dissolves in acidic environments.

For chlorite (see Figure 12a), precipitation is observed from near the wellbore up to around 8m in the reservoir zone with more prominence in the skin zone while further dissolution from its initial volume is observed around the reservoir zone up to around 30m after the lower pH injection (Scenario 3a, 3b, 3c). Beyond 30m, there are no observed changes indicating stable reservoir conditions in terms of chlorite. The switch from neutral brine injection to binary utilization dissolved some of the precipitated chlorite as expected due to a lower pH.

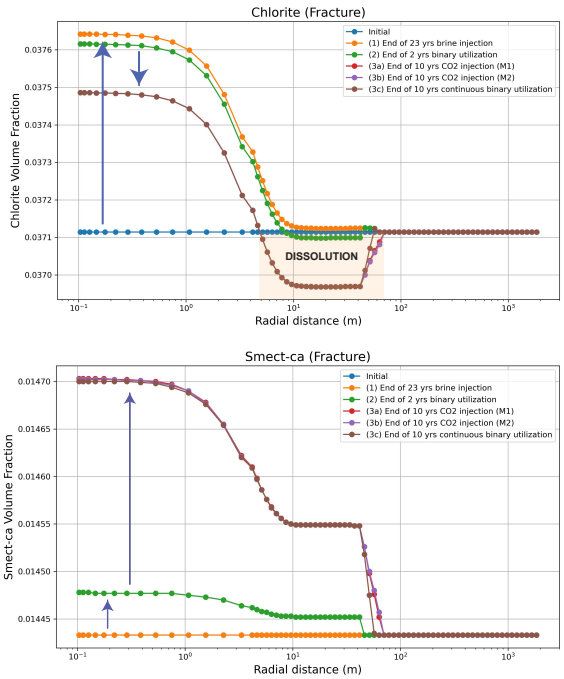


Figure 12. (a) Chlorite and (b) smectite volume fraction changes across the radial distance.

Meanwhile, following binary utilization, smectite mineral volume fraction increased indicating precipitation (see Figure 12b). Since the binary brine injected is acidic, mixing of this fluid to the near neutral in situ water rendered the smectite supersaturated hence precipitation occurred (Ajima et al., 1998), then this precipitation is further enhanced

with the introduction of more CO_2-rich water (Scenario 3a, 3b). The lower pH promotes dissolution of primary minerals leading to precipitation of secondary clay minerals like smectite (Xu et al., 2008). Although minimal, the extent of precipitation is up to around 60m from the wellbore.

Epidote typically forms at temperatures above 200°C and with the injection temperature of 140°C, dissolution is more likely favored but only minimal at a magnitude of 10^{-5}. The lower pH and release of calcium is indicated by increased calcium concentration in the fluid and leads to dissolution of epidote although very minimal in this case. There is a localized dissolution, only limited up to around 40m after binary utilization and CO_2 co-injection forecasts (see Figure 13a). On the other hand, the lower injection temperature reduced quartz solubility hence precipitation occurred, although the magnitude of precipitation is very small in the order of 10^{-6}. While no further changes in the mineral volume fraction across scenarios 1 to 3c.

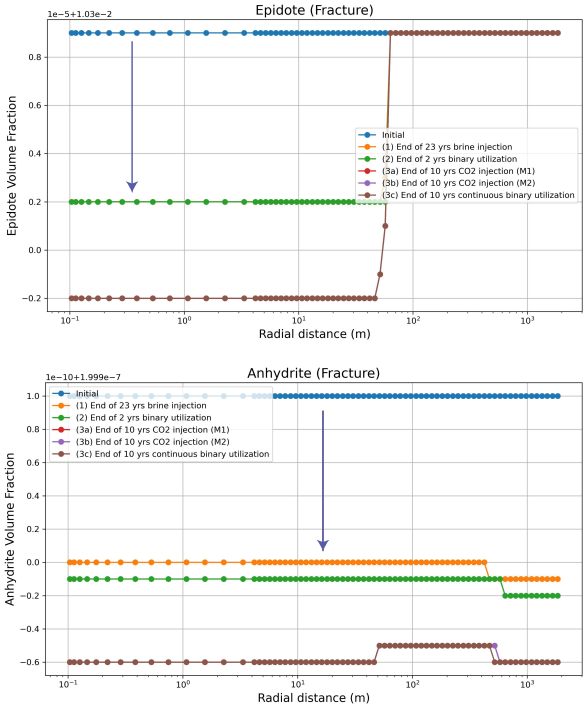


Figure 13. (a) Epidote and (b) anhydrite mineral volume fraction changes.

Anhydrite was not initially present in the feedzone being modelled but it was added to the model input and just set at very low initial mineral volume fraction to see if there was potential changes after the brine injection chemistry changes. As shown in Figure 13b, there is a negligible dissolution in order of 10^{-10} due to colder injection temperatures. Not shown here but there is also a negligible dissolution of illite in the order of 10^{-9}.

While for the rest of the minerals such as amorphous silica, hematite, and goethite, there are no changes observed across all the changes in chemistry and injection temperatures. For amorphous silica, this stability is consistent with suppressed polymerization under low pH conditions.

4. SUMMARY AND CONCLUSIONS

This study investigated the coupled hydraulic and geochemical responses of Well K1 in Mt Apo Geothermal Production Field under long-term neutral brine, binary brine, and a proposed non-condensable gas (NCG)-charged binary brine reinjection using reactive transport modeling in 1D domain.

The 1D radial model was calibrated with the actual downhole pressures at shut and flowing conditions as well as the actual injected chemistry and gave reasonable matches. It captured the near-wellbore dynamics effectively, including permeability increases within a radial distance of up to approximately 60m at the end of neutral brine injection for 23 years and at the end of binary utilization for two years. Whereas permeability increases were up to around 70m at the end of the future scenario of continuous binary utilization for another 10 years while the extent of increase was up to 80m at the end of both future scenarios of NCG-charge binary brine for 10 years (M1 and M2). These changes were more apparent in the fracture (at the maximum of ~10%) than in the matrix. Out of the three future scenarios, results indicate that the NCG-charged binary brine has a greater degree of changes across the radial distance. This is also reflected in the mineral volume evolutions particularly dolomite which had dissolution and smectite which had precipitation, both up to 80m at most.

Calcite undergone dissolution for the first 40m and precipitation from 40m to 900m while chlorite had the opposite with precipitation in the first 50-70m and dissolution up to 650m under CO_2-enriched scenarios, indicating the strong influence of fluid chemistry on reservoir permeability.

Comparing the future scenarios, NCG-charged reinjection resulted in a higher dissolution than purely binary brine reinjection. This indicates that NCG-charged injection could preserve the injection capacity of the well even with the inherent lower binary brine injection temperature which is prone to scaling. However, this study does not include the corrosion potential associated with lower pH injection hence it is recommended to evaluate the pre and post NCG-charged brine chemistry with Fe-CO_2-H_2O stability diagrams. Thus, injecting NCG-charged binary brine shows positive effects in terms of permeability enhancement, porosity evolution, and mineral volume changes with provision of further studies in terms of corrosion risks and execution of the injection strategy. This is to ensure an optimal process that leaves carbon, captured.

ACKNOWLEDGEMENTS

The authors express their gratitude to Energy Development Corporation for permission to publish this work.

REFERENCES

Abd Ghafar, S., Allan, G., Ferguson, A., Siega, F., Rivera, M., & Murphy, B. (2022). Non Condensable Gas Reinjection Trial at Ngatamariki Geothermal Power Plant. In *Proceedings 44th New Zealand Geothermal Workshop. Auckland, New Zealand*.

Adams, M. C., Moore, J. N., Bjornstad, S., & Norman, D. I. (2000). Geologic history of the Coso geothermal system. *Transactions-geothermal resources council*, 205-210.

Ajima, S., Todaka, N., Muratake, H. (1998). An interpretation of smectite precipitation in production wells caused by the mixing of different geothermal fluids. In *Proceedings 23rd Workshop on Geothamal Reservoir Engineering, Standford University (SGP-TR-158)*.

Altar, D. E., & Kaya, E. (2020). Numerical modelling of the interaction between geothermal injectate-non condensable gas solutions and greywacke. *International Journal of Greenhouse Gas Control*, *94*.

Aragon, G. M., & Sambrano, B. M. (2010). Assessment of boiling processes and initial steam fractions of the Mindanao geothermal production field, Philippines. In *Proceedings of the World Geothermal Congress* (pp. 25-29).

Bonafin, J., Pietra, C., Bonzanini, A., & Bombarda, P. (2019, June). CO2 emissions from geothermal power plants: evaluation of technical solutions for CO2 reinjection. In *Proceedings of the European Geothermal Congress*.

Department of Energy (2023). *Key Energy Statistics 2023.* Retrieved from https://legacy.doe.gov.ph/key-energy-statistics-dashboards/total-ghg-emissions

DiPippo, R. (2016). Geothermal Power Generation: Developments and Innovation. Woodhead Publishing. ISBN 978-0-08-100337-4.

Energy Development Corporation (2023). *First Gen-EDC's 2023 Integrated Report*. Retrieved from https://integratedreport.energy.com.ph

Erol, S., Akın, T., Başer, A., Saraçoğlu, Ö., & Akın, S. (2022). Fluid-CO2 injection impact in a geothermal reservoir: Evaluation with 3-D reactive transport modeling. *Geothermics,* 98. https://doi.org/10.1016/j.geothermics.2021.102271

Frassinetti, M., Pezzoni, R., Menghetti, G.R. (2022). Maximizing the Potential of Geothermal Resources in Steam Power Plants with Retrofitted Binary Technology: Exergy's Case Study in the Philippines, Mindanao 3 Power Plant. *Geothermal Resources Council Transactions, 46,* 309-321.

Fridriksson, T., Merino, A.M., Orucu, A. Y., Audinet, P. (2017). Greenhouse Gas Emissions from Geothermal Power Production. In *Proceedings, 42nd Workshop on Geothermal Reservoir Engineering, Stanford University (SGP-TR-212)*.

Kaieda, H., Ueda, A., Kubota, K., Wakahama, H., Mito, S., Sugiyama, K., Tokumaru, T. (2009). Field experiments for studying CO2 sequestration in solid minerals at the Ogachi HDR geothermal site, Japan. In Proceedings 34th Workshop on Geothermal Reservoir Engineering. Stanford University, SGP-TR-187.

Kaieda, H. (2021). Lessons Learned from the Ogachi and Hijori HDR/EGS Projects,

Japan. In Proceedings World Geothermal Congress 2020+1. Reykjavik, Iceland.

Kolar, M., Osgood, S., & Echt, W. (2015). Coso Case Study: 22 Years of Reliable Sulfur Removal. In *GRC Transactions (Vol. 39)*.

Lévy, L., Maurya, P.K., Fiandaca, G., Bording, T.S., Madsen, L.M., Gailler, L., Byrdina, S., Ratouis, T., Tómasdóttir, S., Sigfússon, B., Árnasosson, K. (2021). Geo-electrical Monitoring of H2S Mineralization into Pyrite, upon Re-injection in Basalts at Nesjavellir Geothermal site, Iceland. In *Proceedings World Geothermal Congress 2020+1 Reykjavik, Iceland*.

Malibiran, M.A.O., Zarrouk, S.J. (2014). Modelling Pre and Post Acid Stimulation of Well T4, Mt. Apo Geothermal Field, Philippines. In *Proceedings 36th New Zealand Geothermal Workshop*. *Auckland, New Zealand*.

Mclean, K., & Richardson, I. (2024). Greenhouse gas emissions from New Zealand geothermal power generation in context. In *New Zealand Geothermal Week 2024*.

Palandri, J. L., & Kharaka, Y. K. (2004). *A compilation of rate parameters of water-mineral interaction kinetics for application to geochemical modeling* (No. 2004-1068). US Geological Survey.

Siahaan, Y. (2024). Modelling Non-Condensable Gas Reinjection Geothermal Dynamics in Geothermal Fields: A Case Study of Nga Tamariki, New Zealand. In Proceedings 10th Indonesia International Geothermal Convention & Exhibition 2024.

Sigfússon, B., Arnarson, M.P., Snæbjörnsdóttir, S.O., Karlsdóttirb, M.R., Aradóttira, E.S., Gunnarsson, I. (2018). Reducing emissions of carbon dioxide and hydrogen sulphide at Hellisheidi power plant in 2014-2017 and the role of CarbFix in achieving the 2040 Iceland climate goals. *International Carbon Conference 2018*. *Energy Procedia 146* (2018) 135–145.

Ratouis, T. M. P., Snæbjörnsdóttir, S., Voigt, M. J., Sigfússon, B., Gunnarsson, G., Aradóttir, E. S., & Hjörleifsdóttir, V. (2022). Carbfix 2: A transport model of long-term CO2 and H2S injection into basaltic rocks at Hellisheidi, SW-Iceland. *International Journal of Greenhouse Gas Control,* 114. https://doi.org/10.1016/j.ijggc.2022.103586

Ragnarsdóttir, K.R., Snæbjörnsdóttir, S.O., Bragadóttir, R.B., Aðalsteinsdóttir, N., Ratouis, T., Arnarson, M., Haraldsdó, H.O. (2023). Project Silverstone: Reduction of CO2 emissions by 95% at the Hellisheidi geothermal power plant, SW-Iceland. In *Proceedings World Geothermal Congress 2023 Beijing, China*.

Richardson, I., Misa, T., Mclean, K., Castillo-Ruiz, N., Ferguson, A., Moodabe-Smith, V., Pearl, D., Wootton, D. (2023). Non-Condensable Gas Reinjection at the Te Huka Geothermal Power Plant. *GRC Transactions, Vol. 47*, 2023

Ruiz, N. C., McClean, K., Richardson, I., Misa, T., Ferguson, A., Altar, D.E., & Kaya, E. (2021). Passive NCG reinjection at Te Huka geothermal binary power plant. In Proceedings 43rd New Zealand Geothermal Workshop.

Sevindik, D.B., Erolb, S., Akin, S. (2024). Numerical modeling of the CO2 injection in the Kızıldere geothermal field using multiple inter-well tracer tests. *Geothermics119*(2024)102964.

Sonnenthal, E., Spycher, N., Xu, T., Zheng, L. (2018). TOUGHREACT V3.6-OMP Reactive Transport User Guide. *Lawrence Berkeley National Library, University of California*.

Sonnenthal, E., Spycher, N., Xu, T., & Zheng, L. (2021). TOUGHREACT V4.13-OMP & TReactMech V1.0. *United States*.

Ueda, A., Kuroda, Y., Sugiyama, K., Ozawa, A., Kaieda, H., Kaji, Y., Mito, S., Wakahama, H. (2010). CO2 Sequestration into Hydrothermal System at Ogachi HDR Site. In *Proceedings World Geothermal Congress 2010 Bali, Indonesia*.

Villena, J.P., Alcober, E.H., Jabonilo, R.G., Cruz, D.H., Penaranda, J.R.S., Sanchez, D.R., Guillen, H.V. (2005). Evaluation of the results of the Tongonan-I CO2 gas injection project, Leyte, Philippines. In *Proceedings World Geothermal Congress*.

White, A. F., & Peterson, M. L. (1990). Role of Reactive-Surface-Area Characterization in Geochemical Kinetic Models. *Chemical Modelling of Aqueous System II* (pp. 461–475). *https://doi.org/10.1021/bk-1990-0416.ch035*

Xu, T., Pruess, K., Apps, J. (2008). Numerical studies of fluid-rock interactions in enhanced geothermal systems (egs) with CO2 as working fluid. In *Proceedings, 33rd Workshop on Geothermal Reservoir Engineering, Standford University (SGP-TR-185)*.

Yanagisawa, N. (2010). Ca and CO2 Transport and Scaling in the Hijiori HDR System, Japan. In *Proceedings World Geothermal Congress, 25–29*.

Yücetaş, İ., Ergiçay, N., & Akın, S. (2018). Carbon Dioxide Injection Field Pilot in Umurlu Geothermal Field, Turkey. In *GRC Transactions (Vol. 42)*.